New Journal of Physics
The open access journal for physics

Fluorescence diffraction assisted by Bloch surface waves on a one-dimensional photonic crystal

A Angelini[1,2], E Enrico[2], N De Leo[2], P Munzert[3], L Boarino[2], F Michelotti[4], F Giorgis[1] and E Descrovi[1,5]

[1] Dipartimento di Scienza Applicata e Tecnologia, Politecnico di Torino, Corso Duca degli Abruzzi 24, I-10129 Torino, Italy
[2] Nanofacility Piemonte, Istituto Nazionale di Ricerca Metrologica, Strada delle Cacce, 91, I-10135 Torino, Italy
[3] Fraunhofer Institute for Applied Optics and Precision Engineering IOF, Albert-Einstein-Strasse 7, D-07745 Jena, Germany
[4] Dipartimento di Scienze di Base ed Applicate per l'Ingegneria, SAPIENZA Università di Roma, Via A Scarpa 16, I-00161 Roma, Italy
E-mail: emiliano.descrovi@polito.it

New Journal of Physics **15** (2013) 073002 (13pp)
Received 4 March 2013
Published 2 July 2013
Online at http://www.njp.org/
doi:10.1088/1367-2630/15/7/073002

Abstract. The use of linear and circular subwavelength gratings for improving the fluorescence extraction from organic dyes spotted on the surface of a one-dimensional photonic crystal is demonstrated. The one-dimensional photonic crystal hosting the gratings allows Bloch surface waves (BSWs) to be coupled in the visible range. We provide experimental evidence for the distributed diffraction of BSW-coupled fluorescence that is locally excited using a microscope-based setup. By diffracting the BSW-coupled fluorescence, a significant improvement in the total fluorescence collection is obtained as compared to a flat one-dimensional photonic crystal.

[5] Author to whom any correspondence should be addressed.

Contents

1. Introduction

Surface plasmon-controlled emission (SPCE) is a well-known effect wherein a significant amount of the energy radiated by an emitter in close proximity to a metallic nanostructure is coupled to plasmonic modes [1–3]. In the particular case of a thin metallic film (e.g. gold or silver) on a glass substrate, SPCE typically results in emitted photons leaking into the substrate, at an angle that is larger than the critical angle for the substrate and proportional to the wavevector of the surface plasmon polaritons (SPPs) onto the metallic layer. In order to extract the light from the substrate, it is necessary to couple the substrate itself to a glass prism in the so-called Kretschmann–Raether configuration or to use a microscope objective in a leakage radiation microscope (LRM) configuration. This effect has been exploited in fluorescence-based biosensing applications [4], with an advantageous improvement of the limit of detection [5].

An effect similar to SPCE can be obtained when proper dielectric multilayers (one-dimensional photonic crystals—1DPCs) are used instead of thin metallic layers [6]. Such 1DPCs can be designed in such a way that Bloch surface waves (BSWs) are allowed to propagate at their truncation surface [7, 8]. Similarly to SPPs, BSWs are characterized by an exponentially decaying amplitude in the outer medium. BSWs can be either transverse electric (TE) or transverse magnetic (TM) polarized and can be excited in the well-known Kretschmann–Raether configuration, with coupling angles beyond the critical angle. Accordingly, BSW-coupled emission [9] can be detected in the reverse Kretschmann scheme, as for SPCE [10]. Although BSW-coupled emission provides a well-defined beaming effect, in some fluorescence-based sensing applications [11], it might be desirable to have better control on the extraction of the radiation coupled to BSWs, which would otherwise be trapped in the substrate because of total internal reflection.

In this work, we consider the use of subwavelength diffraction gratings for controlling the extraction of BSW-coupled fluorescence that is locally excited on a patterned 1DPC (figure 1). In the field of plasmonics, this approach has recently been gaining considerable interest, since it opens up new possibilities in photon management at the nanoscale [12–14].

Given some inherent advantages of BSWs over SPPs on metallic films (e.g. lower losses, higher resonance Q factor, lower decoherence, spectral and polarization tunability), we present here a first demonstration of the manipulation of BSW-coupled fluorescence by means of a 1DPC surface patterning. Experimental measurements are conducted with the help of a modified microscope-based setup able to work as an LRM [15]. By considering both the direct plane and

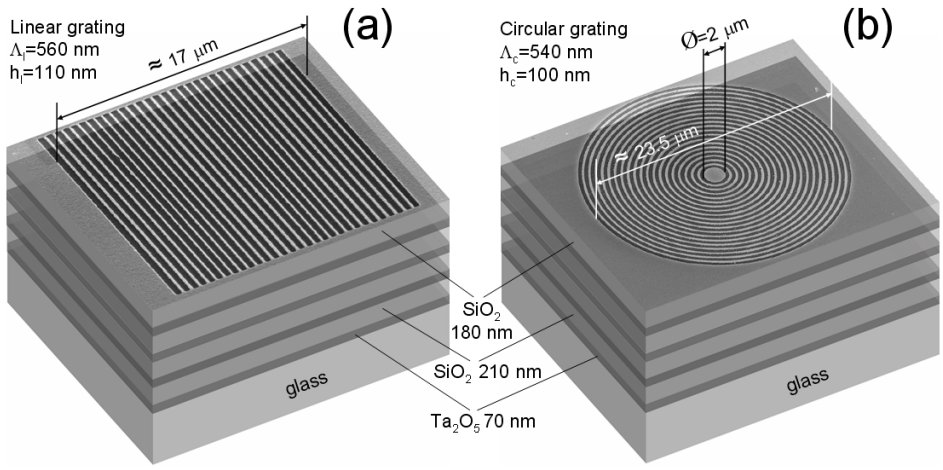

Figure 1. Sketch of the employed 1DPC patterned with either a subwavelength linear grating (a) or a circular grating with a 2 μm inner spacer (b).

the Fourier plane of the imaged field distributions, it is shown that it is possible to collect part of the radiated power leaking through BSW modes by diffracting them normally to the 1DPC surface.

2. Photonic crystal structures

The 1DPC consists of a dielectric multilayer made up of a stack of Ta_2O_5 (high refractive index) and SiO_2 (low refractive index) layers, deposited on a glass coverslip (150 μm thickness) by plasma ion-assisted deposition under high vacuum conditions (APS904 coating system, Leybold Optics). The high and the low refractive index layers have a thickness of 70 and 210 nm, respectively, whereas the SiO_2 top layer is 180 nm thick.

The SiO_2 top layer is directly patterned by focused ion beam (FIB) lithography with either a linear or a circular grating, with a period of $\Lambda_1 = 560$ nm and $\Lambda_c = 540$ nm, respectively. The FIB machining was performed using an FEI Dualbeam Quanta 3D™ equipped with the nanometer pattern generator system by J C Nabity with an acceleration voltage of 30 kV and a current of 50 pA.

The overall depth of the grooves is $h_1 = 110$ nm for the linear grating and $h_c = 100$ nm for the circular grating. The planar 1DPC layout is designed in such a way that TE-polarized (electric field parallel to the multilayer interfaces) BSWs are sustained for wavelengths shorter than 650 nm. The linear and the circular gratings were designed in order to produce a first-order diffraction of BSWs almost normally to the sample surface at wavelengths from 560 to 620 nm. In order to investigate the coupling of fluorescent emitters to BSWs, a solution of 0.5 mg ml^{-1} of rhodamine 6G (R6G) diluted in ethanol was spun on both the bare and the structured 1DPC surface.

3. Results and discussion

The experimental setup is based on a customized microscope mounting consisting of two portions: an upper wide-field microscope and a lower LRM microscope, aligned along the same

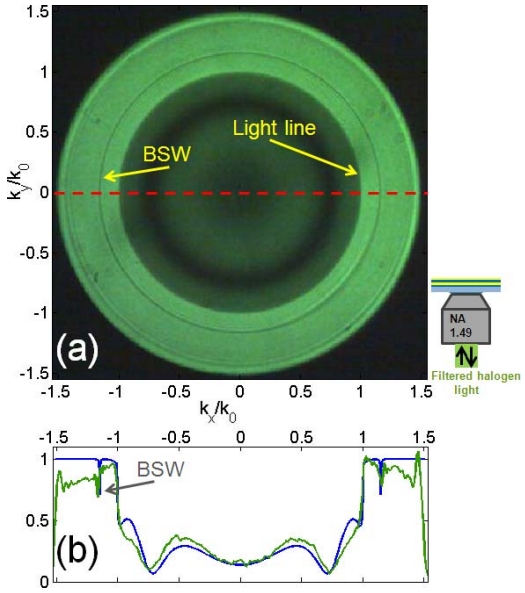

Figure 2. (a) BFP image of the NA = 1.49 objective illuminating a flat 1DPC with incoherent, unpolarized light (filtered at $\lambda = 532 \pm 1$ nm); (b) cross-sectional intensity profile along the red dashed line depicted in (a) (solid green line) and calculated reflectivity profile for an s-polarized plane wave at $\lambda =$ 532 nm (solid blue line).

optical axis. Both microscopes are equipped with an RGB color CMOS camera (DCC1645C from Thorlabs). The upper microscope employs a high numerical aperture objective (NA = 0.95) operating in air (Olympus MPlanAPON 100×), while the lower microscope employs an oil immersion objective with an NA of 1.49 (Nikon APO TIRF 100×). The two microscopes can focus on the same focal plane, where the sample is positioned. The sample can be moved by means of a piezo drive along the three Cartesian directions (100 μm × 100 μm × 20 μm).

The LRM can provide a focal plane or a back focal plane (BFP) image of the oil immersion objective. Thanks to this feature, we can image either the spatial distribution or the angular distribution of the optical fields collected with the oil immersion objective [16]. The high flexibility offered by such a setup allows us to operate in a plurality of configurations for white light/laser illumination/collection, and the possibility of performing fluorescence imaging. In the following, for each presented result, an illustrative sketch of the corresponding microscope configuration employed is shown.

3.1. Flat one-dimensional photonic crystals (1DPCs)

A flat portion of the 1DPC is firstly considered. The lower LRM microscope is used to image the BFP distribution of light reflected by the sample, upon illumination through the oil immersion objective, directly contacted to the glass substrate. Illumination is provided by a quasi-collimated white light halogen source filtered with a laser line filter (MaxLine filter 532, Semrock) transmitting light in the spectral range $\lambda = 532 \pm 1$ nm. The use of incoherent light improves the image quality, avoiding the problems of speckles. Representative results are shown in figure 2.

The image in figure 2(a) indicates the intensity of light reflected under a reflection angle θ such that $n_{\mathrm{obj}} \sin\theta = \sqrt{n_{\mathrm{obj}}^2 \sin^2\theta_x + n_{\mathrm{obj}}^2 \sin^2\theta_y}$, where θ_x and θ_y indicate the leakage directions along the x- and y-axis, respectively, and n_{obj} is the refractive index of the collecting objective. The leakage directions are related to the corresponding wavevector components as $k_x = k_0 n_{\mathrm{obj}} \sin\theta_x$ and $k_y = k_0 n_{\mathrm{obj}} \sin\theta_y$, respectively, where $k_0 = 2\pi/\lambda$ is the modulus of the wavevector in vacuum. The outer circle has a diameter proportional to the NA of the collecting objective. The obtained BFP image shows a sharp increase of the reflected light when the total internal reflection (TIR) condition is achieved, i.e. on a circle with radius $\sqrt{(k_x/k_0)^2 + (k_y/k_0)^2} = n_{\mathrm{obj}} \sqrt{\sin^2\theta_x + \sin^2\theta_y} = 1$ (light cone in air). For leaking directions comprised within the light line in air, the 1DPC is transmissive and light is partially reflected according to the band structure of the multilayer. In the TIR regime, the reflected light is imaged in an annular region limited by an inner radius defined by the light line and an outer radius defined by the objective NA. In such an annular region, the light is distributed homogeneously. At a radius $\sqrt{(k_x/k_0)^2 + (k_y/k_0)^2} = 1.15$, a narrow low-reflectivity dip is found. By comparing the cross-sectional distribution of the BFP intensity along the horizontal dashed line in figure 2(a) with a corresponding angular reflectivity calculated at $\lambda = 532$ nm [17], it is possible to account for the observed dips to the coupling of BSWs (figure 2(b)). The shallow depth of the dip can be explained by recalling that the incident light is unpolarized, while in this case BSWs are allowed in TE-polarization only.

As far as fluorescence is concerned, we illuminate the top surface of the 1DPC with a laser beam ($\lambda = 532$ nm) focused through the upper microscope. Fluorescence imaging is performed by adding an edge filter (Semrock 532 nm RazorEdge) in front of the lower microscope CMOS camera. Figure 3(a) shows the obtained BFP fluorescence image with some residual amount of laser radiation in the center.

Similarly to the well-known SPCE on metallic films, BSW-coupled fluorescence is distributed as a bright ring lying beyond the light line. However, the BSW-coupled fluorescence shows an azimuthally distributed polarization, as opposed to the radial polarization produced in SPCE [18].

In figure 3(a) the dashed green circle indicates the position of BSW coupled at the (excitation) wavelength $\lambda = 532$ nm that has been filtered out by the edge filter.

The color CMOS camera produces a composite image wherein it is possible to separate the light intensities as individually detected by the three R, G and B pixels (RGB spectral sensitivities can be found at www.thorlabs.de/newgrouppage9.cfm?objectgroup_id=4024). Given the emission spectrum of R6G, only the R and G channels are mainly involved in fluorescence detection. In figure 3(b) the cross-sectional profiles of BSW-coupled fluorescence intensities for the G and R channels are shown. A normalization to the maximum of intensity in each channel is performed. As expected, the residual laser light in the center of the BFP affects mainly the intensity profile of the G pixel. More interestingly, the R and G peaks associated with BSWs are spatially shifted on the BFP, as a consequence of the BSW angular/spectral dispersion [9] (see inset for a detailed view).

3.2. Linearly corrugated 1DPCs

Because of their evanescent nature, there is no direct coupling between BSWs and propagating photons in the outer medium (air in the present case). However, a grating can provide additional

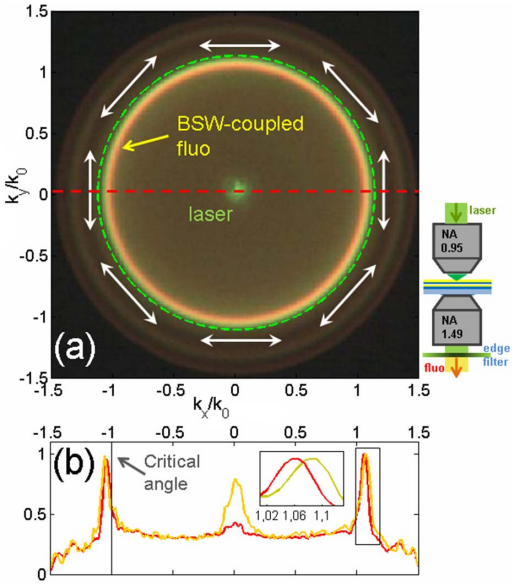

Figure 3. (a) BFP image of the NA = 1.49 objective collecting fluorescence from a flat 1DPC laser illuminated by means of the upper objective; (b) cross-sectional intensity profiles according to the R (solid red line) and G (solid yellow line) camera pixels along the red dashed line depicted in (a). In the inset, the peak displacement is an indication of the BSW-coupled fluorescence dispersion.

momentum for incident light to couple to BSWs through, for example, first-order diffraction. In the past, it has been shown that a subwavelength grating can back-reflect BSWs, thus producing an energy bandgap [19]. In the present case, a linear grating with spatial period $\Lambda_1 = 560\,\text{nm}$ is fabricated onto the 1DPC. When filtered incoherent light ($\lambda = 532\,\text{nm}$) is focused by the upper objective onto the linear grating, a corresponding BFP image of the lower oil-immersion objective is found as shown in figure 4(a).

The inner bright (saturated) circle corresponds to transmitted light as focused by the NA = 0.95 objective. The ± 1 diffraction order of the grating (grating vector $|\bar{K}_{\text{grat}}| = 2\pi/\Lambda_l$ almost parallel to the x-direction) can provide momentum matching to BSWs as demonstrated by the two bright arcs lying beyond the light line. Depicted in figure 4(a) is a vectorial diffraction diagram where $\bar{k}'_{\text{BSW}} = \bar{k}'_{\text{inc}} \pm \bar{K}_{\text{grat}}$, with $\bar{k}'_{\text{BSW}} = \bar{k}_{\text{BSW}}/|\bar{k}_{\text{BSW}}|$ and $\bar{k}'_{\text{inc}} = \bar{k}_{\text{inc}}/|\bar{k}_{\text{inc}}|$. In figure 4(b) the position of the two bright arcs along the dashed red line in the figure corresponds approximately to the BSW reflectivity dips observed on the flat 1DPC (see figure 3(b)). The slight shift of the BSW resonance toward smaller leakage angles is produced by the decrease of the effective refractive index of the top 1DPC layer because of the corrugation [20].

The grating provides a wavevector matching condition for free-space light propagating in air to couple to BSWs at $\lambda = 532\,\text{nm}$. As far as fluorescence emission is concerned, the grating is found to diffract BSW-coupled fluorescence through the -1 diffraction order (figure 5(a)).

Superposed to the bright circle associated with the leakage of BSW-coupled fluorescence, the BFP fluorescence image reveals two additional (polychromatic) bright arcs, mutually intersecting in the center. A similar result has been found for SPCE on periodically corrugated metallic films [21–23] and has been explained as a signature of the diffraction of plasmon-coupled fluorescence. In fact, when the grating vector equals the wavevector of the surface

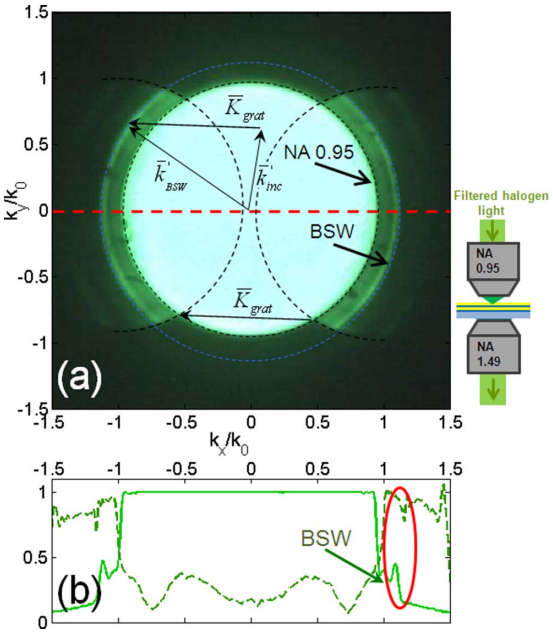

Figure 4. (a) BFP image of the NA = 1.49 objective collecting incoherent light (filtered at $\lambda = 532$ nm) from a linear grating on a 1DPC illuminated by means of the upper objective (NA = 0.95); (b) cross-sectional intensity profile along the red dashed line in (a) (solid light green line) and measured reflectivity profile from figure 2(b) (dashed dark green line). Grating-coupled BSWs are observed as narrow peaks outside the cone of direct illumination and roughly corresponding to the reflectivity dips observed in figure 2(b).

mode wherein the emission is coupled, a normal diffraction may occur normally to the sample surface. In this case, since BSW-coupled fluorescence is leaking isotropically with respect to the xy-plane and the grating is oriented along the x-direction, diffraction only affects the θ_x direction of propagation, through the corresponding wavevector components $k_x = \frac{2\pi}{\lambda} n_{\text{obj}} \sin\theta_x$ for each wavelength λ.

By looking more particularly at the R and G channel intensity profiles presented in figure 5(b) along the $\theta_y = 0$ (dashed) line, the appearance of a central peak is observed. For the G channel, the peak is also due to the residual laser light passing through the edge filter and is not suitable for further considerations on BSW-coupled fluorescence diffraction. Conversely, the R channel is rather insensitive to the residual laser radiation (as shown in figure 3(b)). Given the spectral sensitivity of the R channel and the R6G emission spectrum [6], we can restrict our attention to the spectral range 580–620 nm and apply the Bragg equation for a $\Lambda_1 = 560$ nm grating. For a given wavelength λ, we find that $k_x^{(-1)}|_\lambda = k_x^{\text{BSW}}|_\lambda - \frac{2\pi}{\Lambda_1}$ results in an overall angular range $\Delta\theta_x \cong 6^\circ$ associated with the -1 diffraction order of BSW-coupled fluorescence.

The experimental findings well match theoretical predictions obtained with a simple two-dimensional finite element numerical model (FEM). Here, a radiating dipole source having dipole momentum normal to the xy-plane is placed on the 1DPC and surrounded by a periodic corrugation with $\Lambda_1 = 560$ nm. The dipole source is radiating in a spectral range 580–620 nm. Starting from the spatial distribution of the s-polarized electromagnetic field energy density

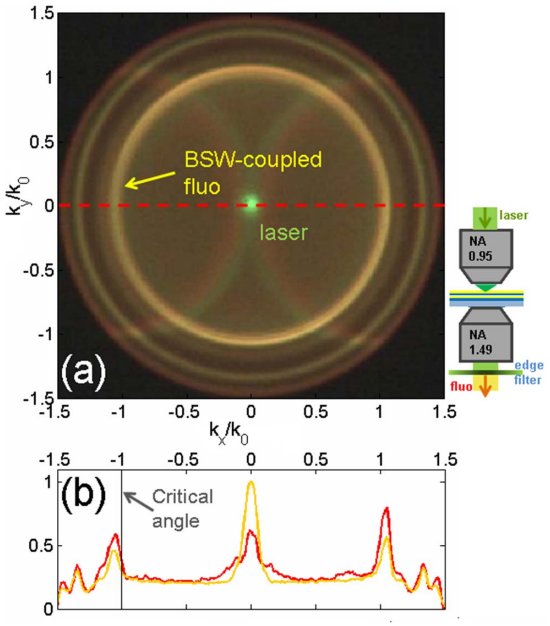

Figure 5. (a) BFP image of the NA = 1.49 objective collecting fluorescence from a linear grating on a 1DPC laser illuminated by means of a top objective NA = 0.95; (b) cross-sectional intensity profiles according to the R (solid red line) and G (solid yellow line) camera pixels along the red dashed line depicted in (a): the central maximum in the G channel relates mainly to a residual laser radiation passing through the edge filter.

obtained in the calculation domain, a far-field angular distribution of the power emitted in the glass substrate is then estimated using commercial software[6] implementing a code based on the surface equivalent theorem [24] from the Kirchoff–Helmholtz integral representation of the field.

In figure 6(a) the spatial distribution of the electromagnetic energy density is calculated for a dipole emitting at $\lambda = 600$ nm. Because of the dipole orientation, the radiated electromagnetic field will be s-polarized (electric field normal to the *xy*-plane). According to the coupling length of BSWs, a fraction of the radiation is directly emitted in the substrate and in the outer medium (air). Moreover, a significant amount of the radiated energy couples with BSWs and propagates along the 1DPC surface. During propagation, BSW-coupled fluorescence is attenuated because of two leakage mechanisms: radiation into the glass substrate and diffraction from the grating. In the far field, this results in directional emission. When a dipole emitting in a spectral range 580–620 nm is considered, an angular distribution of the integral power emitted in the substrate can be calculated (figure 6(b)). A weighting on the spectral sensitivity of the R channel of the CMOS camera is performed in order to allow a direct comparison with experiment. The central peak, associated with BSW diffraction, shows a maximum of intensity at 0° that is comparable with the BSW leakage peak intensities, thus confirming the experimental findings shown in figure 5(b). The specific orientation of the dipole is such that no significant emission angles other than those related to BSW leakage and diffracted BSW are present. Nevertheless, as

[6] COMSOL Multiphysics 4.2a, RF module.

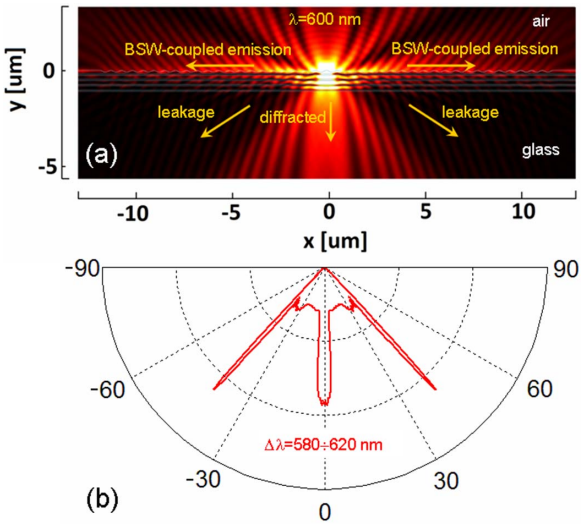

Figure 6. (a) FEM calculation of the electromagnetic field intensity produced by a radiating dipole source (dipole momentum normal to the *xy*-plane, emission wavelength $\lambda = 600$ nm) surrounded by a linear grating; (b) far-field angular distribution of integral emitted power leaking in the glass substrate in the spectral range 580–620 nm.

more general dipole orientations are considered, the final result is a weighted average of all the possible mode-coupled emission leaking in the substrate. Experimentally, it was not possible to control the orientation of emitters and it is therefore interesting to note that the additional bright rings in figure 5(a) that are external to the BSW ring are related to fluorescence coupling into p-polarized modes sustained by the 1DPC.

3.3. Circularly corrugated 1DPCs

In order to overcome the anisotropy of diffraction produced by a linear grating, a circular corrugation ($\Lambda_c = 540$, $h_c = 100$ nm) is considered. Furthermore, the structure has an inner disc spacer of diameter 2 μm.

With an incoherent light illumination ($\lambda = 532$ nm) focused through the upper objective (NA = 0.95), the circular grating couples the incident radiation to BSWs isotropically in the *xy*-plane (figure 7(a)), provided that the spot light is large enough to lighten the whole grating. As for the linear grating, the intensity profile along a horizontal cross section (dashed red line in figure 7(a)) reveals two BSW leakage peaks corresponding to the BSW reflectivity dips observed on the flat 1DPC in figure 2(b). Also in this case, the grating provides enough additional momentum to free-space photons propagating in air to couple to surface modes.

The fluorescence outcoupling is investigated by imaging the direct object plane through the oil-immersion objective. Fluorescence excitation is performed by focusing the laser beam on the inner circular spacer, by means of the upper objective (NA = 0.95). The obtained spot size is such that it is completely contained within the central spacer, as shown in the bright-field image of figure 8(a). The fluorescence image shown in figure 8(b) reveals a central bright spot from where fluorescence directly radiates in the substrate. More interestingly,

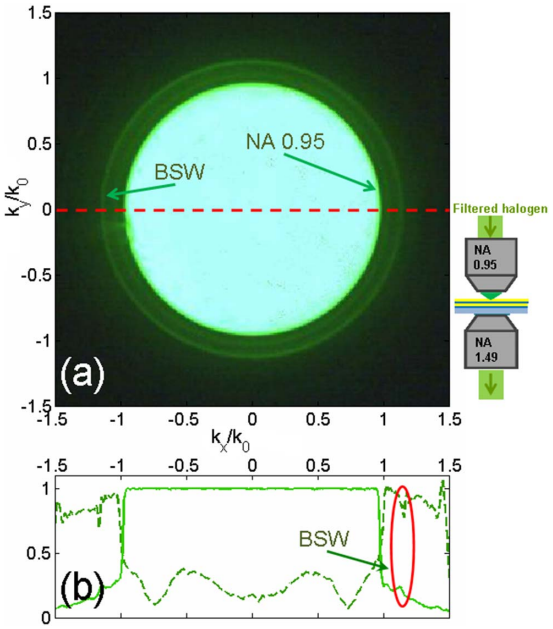

Figure 7. (a) BFP image of the NA = 1.49 objective collecting light from a circular grating on a 1DPC illuminated with unpolarized, incoherent light (filtered at $\lambda = 532$ nm) by means of a top objective NA = 0.95; (b) cross-sectional intensity profile along the red dashed line depicted in (a) (solid light green line) and measured reflectivity profile from figure 2(b) (dashed dark green line). Grating-coupled BSWs are observed as narrow peaks outside the cone of direct illumination.

fluorescence is also detected in the surrounding of the region of direct excitation, with an intensity that is radially decreasing as we move away from the grating center. Such a distributed fluorescence is outcoupled in the substrate thanks to a mechanism of diffraction of BSW-coupled radiation.

We observe here evidence of the delocalization of collected fluorescence far away from the original location of the excited emitters. This effect has also been found for surface plasmons over a smaller length scale, and critically considered in SPP-mediated imaging [25, 26].

Generally, surface modes can represent an efficient 'drain' channel for radiation leaking into the substrate. The use of the presented diffraction gratings can recover a significant portion of this surface mode-coupled fluorescence by outcoupling it normally to the 1DPC surface. As a result, an increase in the overall amount of collected fluorescence is obtained, as compared to the case wherein only the area of direct illumination is considered. In fact, if we integrate the fluorescence intensity, as detected by the R and G camera pixels separately, over the directly illuminated region and over the whole grating region outside the inner spacer, we find that the latter exceeds the former by a factor of about 20 times.

4. Summary

Extensive experimental work on the use of linear and circular gratings for diffracting BSW-coupled fluorescence has been presented. By following an analogy to the plasmonic SPCE, we

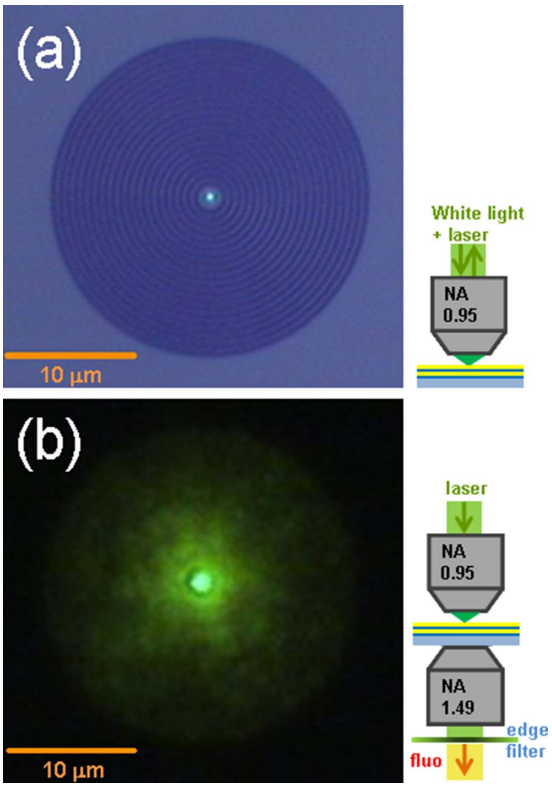

Figure 8. (a) Reflection bright-field image of a circular grating made through a top objective (NA = 0.95) and laser focusing in the central spacer; (b) direct plane image of fluorescence collected by the NA = 1.49 objective

introduced the concept of BWS-coupled directional leakage of fluorescence radiated by emitters located on the surface of properly designed 1DPCs.

Furthermore, we showed how such a 'reservoir' of emitted power coupled to BSWs can be successfully manipulated by exploiting diffraction effects described by the classical grating theory. In particular, we demonstrated that BSW-coupled emission can be extracted through diffraction normally to the 1DPC surface. Such a diffracted BSW-coupled fluorescence has spatially distributed characteristics, involving spatial regions far away from the location of direct excitation. One advantage of the presented approach is the increase of the overall fluorescence intensity that can be collected from the surrounding of a focused laser spot used for fluorescence excitation.

The proposed approach paves the pathway for exploiting BSWs on 1DPCs as a dielectric analogue of surface plasmons for fluorescence enhancement useful, for example, in biosensing applications based on fluorescent markers.

Acknowledgments

We acknowledge the collaboration with NanoFacility Piemonte, INRiM, a laboratory supported by Compagnia di San Paolo. This research has received funding from the European Union Seventh Framework Programme (FP7/2007–2013) under grant agreement no. 318035—Project BILOBA.

References

[1] Lakowicz J R 2006 *Principles of Fluorescence Spectroscopy* 3rd edn (New York: Springer)

[2] Liebermann T and Knoll W 2000 Surface-plasmon field-enhanced fluorescence spectroscopy *Colloids Surf.* A **171** 115–30

[3] Lakowicz J R, Ray K, Chowdhury M, Szmacinski H, Fu Y, Zhang J and Nowaczyk K 2008 Plasmon-controlled fluorescence: a new paradigm in fluorescence spectroscopy *Analyst* **133** 1308–46

[4] Cao S H, Cai W P, Liu Q and Li Y Q 2012 Surface plasmon-coupled emission: what can directional fluorescence bring to the analytical sciences? *Annu. Rev. Anal. Chem.* **5** 317–36

[5] Cao S H, Xie T T, Cai W P, Liu Q and Li Y Q 2011 Electric field assisted surface plasmon-coupled directional emission: an active strategy on enhancing sensitivity for DNA sensing and efficient discrimination of single base mutation *J. Am. Chem. Soc.* **133** 1787–9

[6] Liscidini M, Galli M, Shi M, Dacarro G, Patrini M, Bajoni D and Sipe J E 2009 Strong modification of light emission from a dye monolayer via Bloch surface waves *Opt. Lett.* **34** 2318–20

[7] Yeh P, Yariv A and Hong C S 1977 Electromagnetic propagation in periodic stratified media: I. General theory *J. Opt. Soc. Am.* **67** 423–38

[8] Gaspar-Armenta J A, Villa F and López-Ríos T 2003 Surface waves in finite one-dimensional photonic crystals: mode coupling *Opt. Commun.* **216** 379–84

[9] Ballarini M, Frascella F, Michelotti F, Digregorio G, Rivolo P, Paeder V, Musi V, Giorgis F and Descrovi E 2011 Bloch surface waves-controlled emission of organic dyes grafted on a one-dimensional photonic crystals *Appl. Phys. Lett.* **99** 043302

[10] Gryczynski I, Malicka J, Gryczynski Z and Lakowicz J R 2004 Radiative decay engineering 4. Experimental studies of surface plasmon-coupled directional emission *Anal. Biochem.* **324** 170–82

[11] Toma K, Descrovi E, Toma M, Ballarini M, Mandracci P, Giorgis F, Mateescu A, Jonas U, Knoll W and Dostalek J 2013 Bloch surface wave-enhanced biosensor *Biosens. Bioelectron.* **43** 108–14

[12] Gómez Rivas J, Vecchi G and Giannini V 2008 Surface plasmon polariton-mediated enhancement of the emission of dye molecules on metallic gratings *New J. Phys.* **10** 105007

[13] Aouani H, Mahboub O, Devaux E, Rigneault H, Ebbesen T W and Wenger J 2011 Plasmonic antennas for directional sorting of fluorescence emission *Nano. Lett.* **11** 2400–6

[14] Jun C Y, Huang K C Y and Brongersma M L 2011 Plasmonic beaming and active control over fluorescent emission *Nature Commun.* **2** 283

[15] Ballarini M, Frascella F, Enrico E, Mandracci P, De Leo N, Michelotti F, Giorgis F and Descrovi E 2012 Bloch surface waves-controlled fluorescence emission: coupling into nanometer-sized polymeric waveguides *Appl. Phys. Lett.* **100** 063305

[16] Zhang D G, Yuan X C, Yuan G H, Wang P and Ming H 2010 Directional fluorescence emission characterized with leakage radiation microscopy *J. Opt.* **12** 035002

[17] Descrovi E, Sfez T, Quaglio M, Brunazzo D, Dominaci L, Michelotti F, Herzig H P, Martin O J F and Giorgis F 2010 Guided Bloch surface waves on ultrathin polymeric ridges *Nano Lett.* **10** 2087–91

[18] Grandidier J, Colas des Francs G, Massenot S, Bouhelier A, Markey L, Weeber J C and Dereux A 2010 Leakage radiation microscopy of surface plasmon coupled emission: investigation of gain assisted propagation in an integrated plasmonic waveguide *J. Microsc.* **239** 167–72

[19] Descrovi E, Giorgis F, Dominici L and Michelotti F 2008 Experimental observation of optical bandgaps for surface electromagnetic waves in a periodically corrugated one-dimensional silicon nitride photonic crystal *Opt. Lett.* **33** 243–5

[20] Sfez T *et al* 2010 Bloch surface waves in ultrathin waveguides: near-field investigation of mode polarization and propagation *J. Opt. Soc. Am.* B **27** 1617–25

[21] Regan C J, Krishnan A, Lopez-Boada R, Grave de Peralta L and Bernussi A A 2011 Direct observation of photonic Fermi surfaces by plasmon tomography *Appl. Phys Lett.* **98** 151113

[22] Regan C J, Grave de Peralta L and Bernussi A A 2012 Equifrequency curve dispersion in dielectric-loaded plasmonic crystals *J. Appl. Phys.* **111** 073105

[23] Chen Y K, Zhang D G, Wang X X, Liu C, Wang P and Ming H 2012 Launching plasmonic Bloch waves with excited dye molecules *Nanotechnology* **23** 475202

[24] Taflove A and Hagness S C 2005 *Computational Electrodynamic: The Finite Difference Time Domain Method* 3rd edn (Boston MA: Artech House) p 329

[25] Guebrou Aberra S, Laverdant J, Symonds C, Vignoli S and Bellessa J 2012 Spatial coherence properties of surface plasmon investigated by Young's slit experiment *Opt. Lett.* **37** 2139–41

[26] Guebrou Aberra S, Laverdant J, Symonds C, Vignoli S, Bessueille F and Bellessa J 2012 Influence of surface plasmon propagation on leakage radiation microscopy imaging *Appl. Phys. Lett.* **101** 123106